Electronic Supplementary Information

Temperature-Regulated Reversible Transformation of Spinel-to-Oxyhydroxide Active Species for Electrocatalytic Water Oxidation

Tingli Zhou[‡], Changhong Wang[‡*], Yanmei Shi[*], Yu Liang, Yifu Yu, and Bin Zhang[*]

Department of Chemistry, School of Science, Institute of Molecular Plus, Tianjin University, Tianjin 300072, China

Experimental Details

1.1 Chemicals. Nickel nitrate ($Ni(NO_3)_2 \cdot 6H_2O$) was purchased from Tianjin Yuanli Chemical Co., Ltd. Cobalt (Ⅱ) nitrate hexahydrate ($Co(NO_3)_2 \cdot 6H_2O$) was purchased from Tianjin Kermel Chemical Reagent Co., Ltd. Ammonium fluoride (NH_4F) and hexamethylenetetramine were obtained from Tianjin Guangfu Technology Development Co., Ltd. Urea ($CO(NH_2)_2$) was purchased from Li Anlong Bohua (Tianjin) Pharmaceutical Chemical Co., Ltd. Potassium hydroxide (KOH) was purchased from Aladdin Ltd. (Shanghai, China). Deionized was used in all the experimental processes. All chemicals were analytical grade and used without further purification.

1.2 Synthesis of $NiCo_2O_4$-Ti. The $NiCo_2O_4$ nanorods array was synthesized according to the reported literature. In a typical procedure, a piece of Ti sheet (about 1×3 cm^2) was soaked in 1.0 M HCl for 15 minutes to remove organic molecules and oxide layer on the surface, then washed with ethanol and deionized water, respectively, and dried at room temperature. After 0.2 mmol $Ni(NO_3)_2 \cdot 6H_2O$, 0.4 mmol $Co(NO_3)_2 \cdot 6H_2O$, 1 mmol NH_4F and 2.5 mmol $CO(NH_2)_2$ were dissolved in 12 mL deionized water in a 20 mL Teflon-lined stainless-steel autoclave, one piece of freshly-treated Ti sheet was added. The autoclave was sealed and treated at 120 ºC for 5 h at a heating rate of 2 ºC min^{-1}, and then allowed to cool down to room temperature naturally. The pink as-coprecipitated (denoted as NiCo hydroxide) was obtained by rinsing with deionized water, alcohol and drying in a vacuum oven. The NiCo hydroxide was then calcined at 350 ºC for 3 h at a heating rate of 2 ºC min^{-1} in air to produce $NiCo_2O_4$ supported on Ti sheet (denoted as $NiCo_2O_4$-Ti).

1.3 Synthesis of $Ni(OH)_2$ nanosheet array. $Ni(OH)_2$ nanosheet array was synthesized according to our previously reported method.[1] In a typical procedure, 2.5 mmol $Ni(NO_3)_2 \cdot 6H_2O$ and 5 mmol hexamethylenetetramine were dissolved in 18 mL distilled water under magnetic stirring. The resulting solution and one piece of freshly-treated

Ti sheet were transferred to a 20 mL Teflon-lined stainless-steel autoclave and maintained at 100 °C for 10 h. The green $Ni(OH)_2$ nanosheet array (denoted as $Ni(OH)_2$-Ti) was obtained by rinsing with deionized water, alcohol and drying in a vacuum oven.

1.4 Materials characterization: All electrochemical measurements were performed on an electrochemical workstation (CHI 660D, CH Instruments, Austin, TX) in a typical three-electrode system. 1.0 M KOH was used as electrolyte for electrochemical measurements, and degassed by bubbling oxygen for 30 min before the measurements. Glassy carbon rod electrode and Hg/HgO electrode with inner reference electrolyte of 1.0 M KOH were used as the counter and reference electrode, respectively. If without extra statement, all the mentioned potentials were against reversible hydrogen electrode (RHE). All the data appeared in electrochemical section was iR corrected, which yielded the relation E (V vs. RHE) = E (V vs. Hg/HgO) + E^{θ} (Hg/HgO) + 0.059 pH iR. (Note: E^{θ} (Hg/HgO) = 0.098 V, the effect of temperature on E^{θ} (Hg/HgO) is negligible). Polarization data was collected at a sweep rate of 10 mV s^{-1}. The Chrono potentiometric curve was measured at 1.608 V vs. RHE for OER to examine the electrochemical stability of $NiCo_2O_4$-Ti without and with heating.

1.5 *In situ* Raman spectroscopy. Raman spectroscopy was recorded on the aforementioned confocal Raman microscope under controlled potentials by electrochemical workstation. The electrolytic cell was homemade by Teflon with a piece of round quartz glass as cover to protect the objective. The $NiCo_2O_4$ and $Ni(OH)_2$ as working electrode were inserted through the wall of the cell to keep the plane of working electrode perpendicular to the incident laser. Prior to the measurements, the working electrodes were carefully covered with epoxy and Teflon tape to ensuring exposed area of 0.25 cm^2. Pt wire as the counter electrode was rolled to a circle around the working electrode. Hg/HgO electrode with inner reference electrolyte of 1.0 M KOH was used as the reference electrode. The maximum applied potential was

carefully controlled for different samples to keep the current density less than 1 mA cm^{-2} in case of too many generated bubbles blocking the light pathway.

1.6 The concentration of surface active sites from the redox features in cyclic voltammetry. Calculated area for $NiCo_2O_4$-45 ºC associated with the reduction of Ni^{3+} to Ni^{2+} = 0.0366 V•A

Hence, the surface concentration of Ni for $NiCo_2O_4$-45 ºC that participated in OER = 0.0366 V • A / (0.1 V S^{-1}×1.602×10^{-19} C×1)= 2.285×10^{18}.

In the same way, the surface concentration of Ni for $NiCo_2O_4$-25 ºC = 0.0251 V•A / (0.1 V S^{-1}×1.602×10^{-19} C×1) = 1.566×10^{18}.

1.7 Determination of Turnover Frequency (TOF) from OER current density. TOF in our study was calculated assuming that the surface active Ni atoms in the redox reaction only participated in OER electrocatalysis. The following equation is,

$$TOF = \frac{j \times A}{Z \times F \times n}$$

where *j* stands for the current density (A cm^{-2}), *z* is the number of electrons transferred to evolve a molecule of product (for O_2, it is 4), *F* is the Faraday constant (96485 C mol^{-1}).

2. Materials Characterization and Performance

2.1 Tafel slopes of $NiCo_2O_4$

As displayed in Fig. S1, the Tafel slope of $NiCo_2O_4$-45 ºC is 68 mV dec^{-1}, which is decreased 16 mV dec^{-1} than that $NiCo_2O_4$-25 ºC.

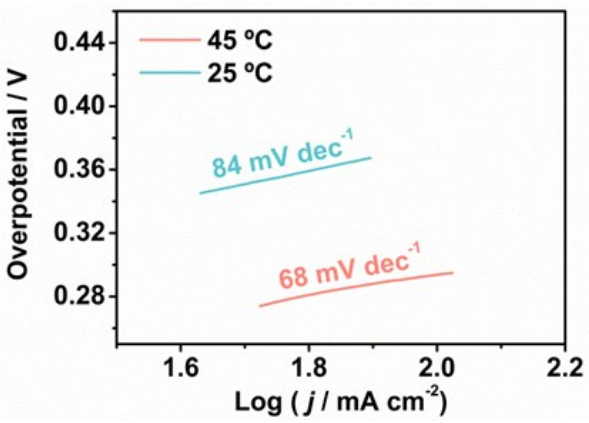

Fig. S1. Tafel slopes of $NiCo_2O_4$ at 25 ºC and 45 ºC measured in 1 M KOH electrolyte.

2.2 Cyclic voltammetry (CV) curves and the area of redox features of $NiCo_2O_4$

As shown in Fig. S2a, we test CV curves of $NiCo_2O_4$ at 25 ºC and 45 ºC in order to calculate the surface active sites. From the area of redox features we can find that the number of surface active sites of $NiCo_2O_4$-45 ºC is more than $NiCo_2O_4$-25 ºC (Fig. S2b and Fig. S2c).

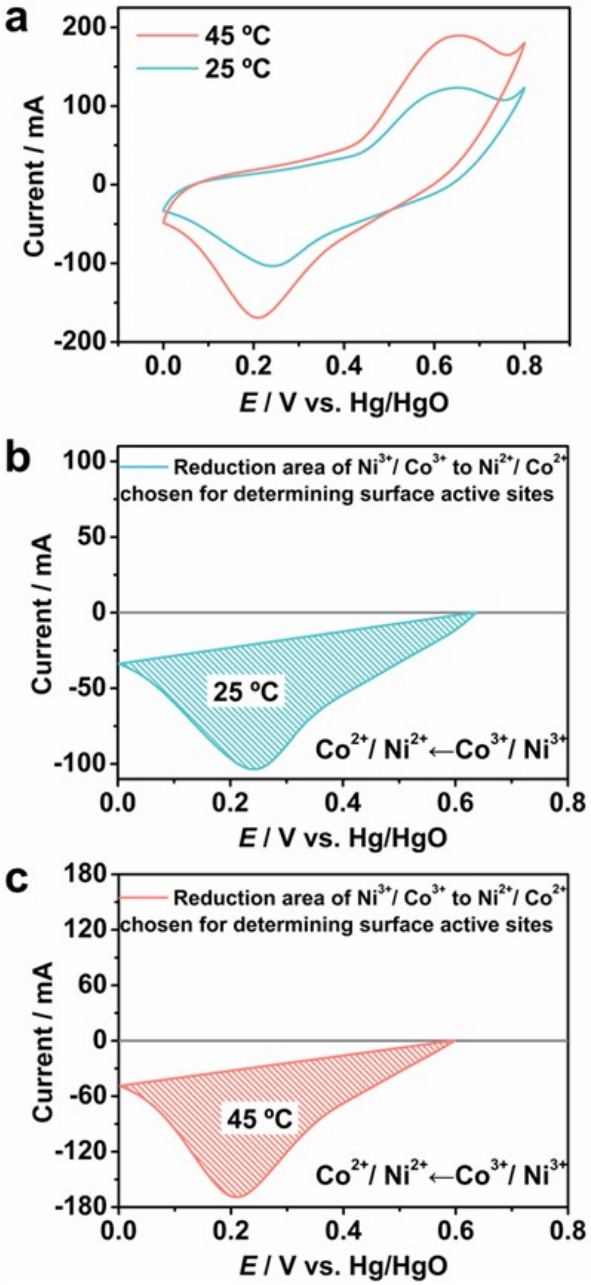

Fig. S2. (a) Cyclic voltammetry (CV) curves of $NiCo_2O_4$ at 25 ºC and 45 ºC measured in 1 M KOH electrolyte. (b) and (c) are the area of redox features of $NiCo_2O_4$ at 25 ºC and 45 ºC for the calculation of surface active sites.

2.3 The turnover frequency (TOF) of $NiCo_2O_4$

As shown in Fig. S3, the TOF value of $NiCo_2O_4$-45 ºC at the overpotential of 300 mV is 0.107 s^{-1}, which is almost 7-times as high as that of $NiCo_2O_4$-25 ºC (0.016 s^{-1}).

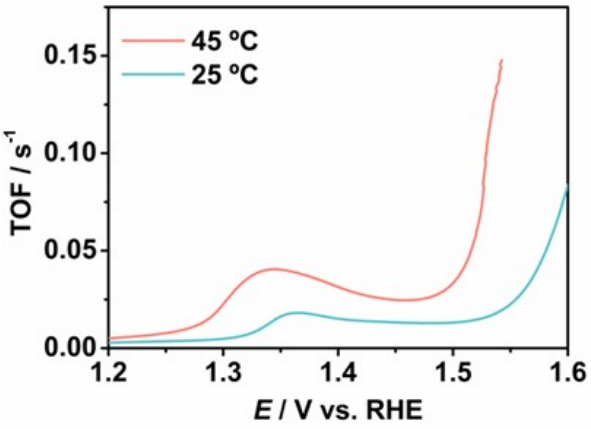

Fig. S3. TOF of $NiCo_2O_4$ at 25 ºC and 45 ºC calculated at various potentials.

2.4 Time-dependent current density curve of $NiCo_2O_4$

Fig. S4 shows the stability of $NiCo_2O_4$ at 25 ºC during OER measurements. It shows that $NiCo_2O_4$ is a catalyst with good stability.

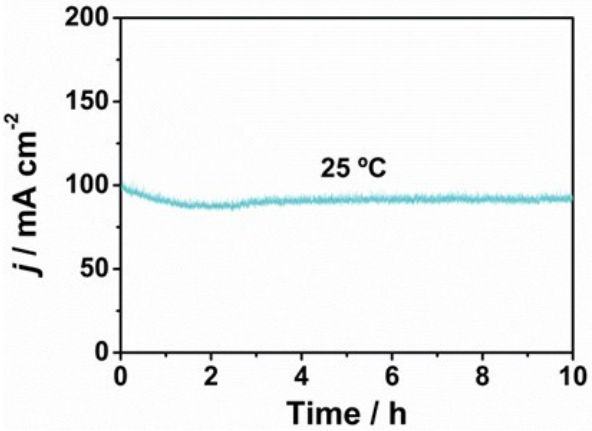

Fig. S4. The time-dependent current density curve of $NiCo_2O_4$ at 25 ºC measured in 1 M KOH electrolyte.

2.5 SEM, TEM images and XRD pattern of $NiCo_2O_4$ after stability test

Compared with the corresponding characterization results which were tested before the OER measurements, the almost identical morphology and crystal confirm the high stability of $NiCo_2O_4$ at 45 ºC (Fig. S5).

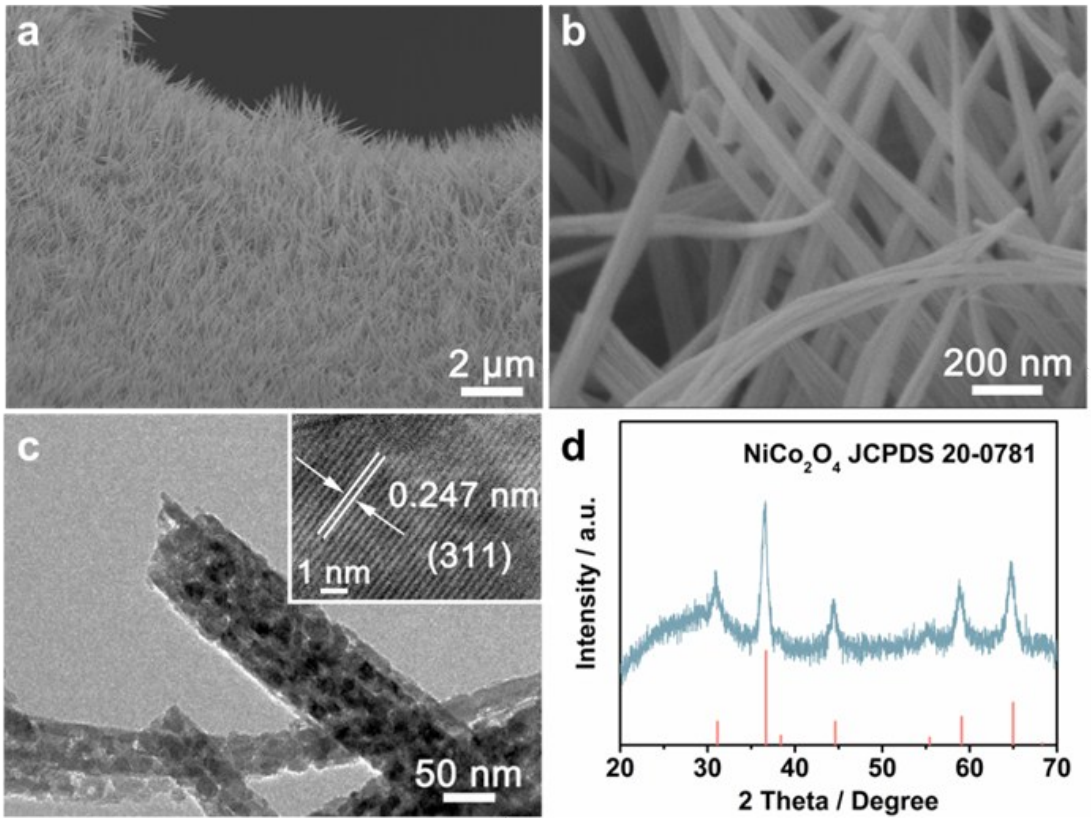

Fig. S5. Characterizations of $NiCo_2O_4$ after stability test at 45 ºC. (a) Low-magnification SEM image and (b) SEM image. (c) TEM (inset: HRTEM) images. (d) XRD patterns of $NiCo_2O_4$ powder.

2.6 *In situ* Raman spectra of $NiCo_2O_4$ after long-term test. And even after long-term test at 25 °C, no peak attributed to NiOOH can be found, further confirming the active species is $NiCo_2O_4$ itself at room temperature (Fig. S6).

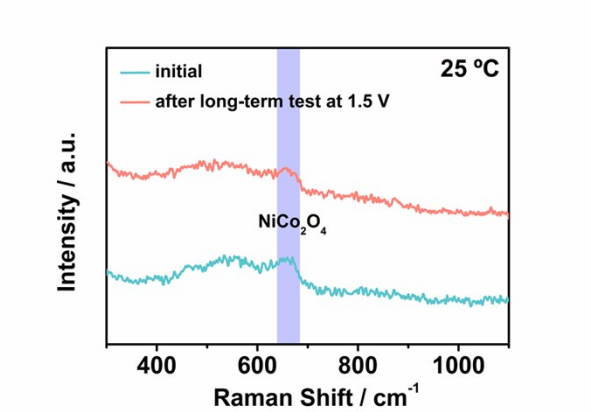

Fig. S6. *In situ* Raman spectra of $NiCo_2O_4$ after long-term test at 25 °C.

2.7 XPS analysis of $NiCo_2O_4$ before and after heating electrochemical OER measurements

In the Ni 2p spectrum of $NiCo_2O_4$ (Fig. S7b), two peaks at 855.4 and 872.6 eV are associated with Ni $2p_{3/2}$ and Ni $2p_{1/2}$. The intense satellite peaks at 861.2 and 879.6 eV indicate the Ni^{2+} cations abound in the sample. The fitting analysis result of Co 2p peak shows two oxidation states identified as Co^{2+} and Co^{3+} (Fig. S7c). The peaks at 779.4 and 794.6 eV in the Co 2p spectrum correspond to Co^{3+} and the peaks at 781.2 and 796.2eV belong to Co^{2+}. It demonstrates that the electron couples Ni^{2+}/Ni^{3+} and Co^{2+}/Co^{3+} are co-existing in the $NiCo_2O_4$. Besides, there are two small satellite peaks at 789.2 and 803.7 eV. In the O 1s spectrum (Fig. S7d), two peaks at 529.5 and 531.0 eV are attributed to surface lattice oxygen and surface adsorption oxygen, respectively. After stability test at heating condition, both the ratios of Ni^{3+} and Co^{3+} increase, indicating the formation of small amount of Ni(Co)OOH, which is in accordance with the results from *in situ* Raman spectroscopy and XAS.

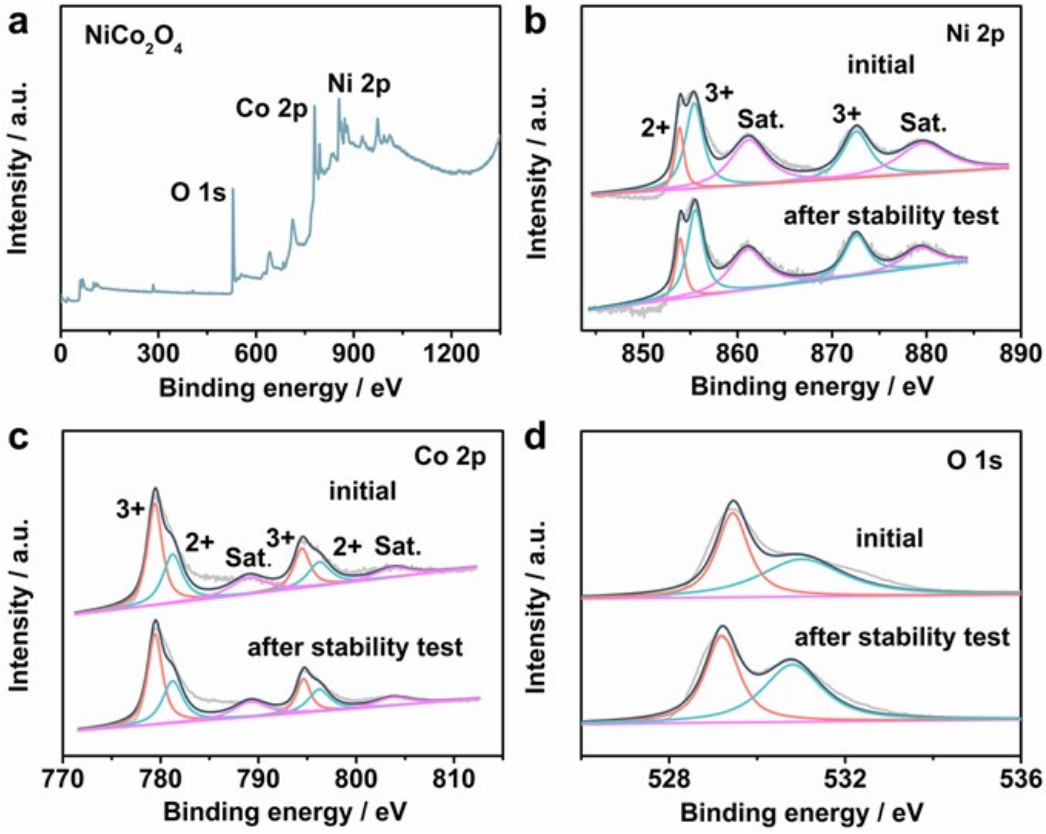

Fig. S7. (a) The XPS survey spectra of $NiCo_2O_4$. (b) Ni 2p spectra, (c) Co 2p spectra and (d) O 1s spectra before and after heating electrochemical OER measurements.

3. Computational methods

Density functional theory (DFT) calculations with plane-wave basis were performed as implemented in Vienna ab initio Simulation Package (VASP).[2] Projector augmented wave (PAW) pseudo-potentials were used.[3] The exchange-correlation contributions to the total energy was estimated by the generalized gradient approximation (GGA) with Perdew-Burke-Ernzerhof (PBE) form.[4] The Hubbard U approach (DFT + U) was adopted to better describe the on-site coulomb correlation of the localized 3d electrons for transition metals with U - J = 3.0 eV for both Ni and Co.[5] An empirical dispersion corrected DFT method (DFT-D2) was carried out to reasonably describe the weak long-distance van der Waals (vdWs) effects.[6] A kinetic-energy cutoff of 500 eV was used. During geometry optimizations, the maximum force on each atom was less than 0.05 eV/Å.[7] The total energy convergence criterion was set as 10^{-4} eV. Spin polarization was considered in all calculations.

Inverse spinel $NiCo_2O_4$ (311) surface was modeled by a p(1 × 3) slab with a thickness of 7.3 Å. A vacuum layer of 15 Å was adopted along the c direction to avoid periodic image interactions. For structural relaxation, the bottom atomic layer was fixed and all other atoms and adsorbates were fully relaxed. The Brillouin zone was sampled by gamma centered k-points mesh of 2×4×1. The β-NiOOH and CoOOH slabs were modeled by one (001) layer with edge Ni or (and) Co exposed. A vacuum layer of 15 Å was adopted along the c direction and the Brillouin zone was sampled by 8×2×1.

The OER under alkaline condition consists of four elementary reaction steps, each involving an electron transfer to the electrode.[8]

$$OH^- + * \rightarrow HO^* + e^- \quad (1)$$

$$OH^- + HO^* \rightarrow O^* + H_2O + e^- \quad (2)$$

$$OH^- + O^* \rightarrow HOO^* + e^- \quad (3)$$

$$OH^- + HOO^* \rightarrow * + O_2 + H_2O + e^- \quad (4)$$

To express the thermochemistry of the sub-reactions of OER, the computational hydrogen electrode (CHE) model proposed by Nørskov and co-workers was used.[9] The free energy change of each step was calculated using the following Equation:

$$\Delta G_i = \Delta E_i + \Delta ZPE_i - T\Delta S_i$$

where i = 1, 2, 3, 4 corresponds to each step in OER. ΔE is the reaction energy, ΔZPE is the change of zero-point energy, T (298.15 K) is temperature, ΔS is the difference in entropy.[10-11]

The theoretical overpotential was given as follows:

$$\eta = \frac{Max[\Delta G_i]}{e} - 1.23\ V$$

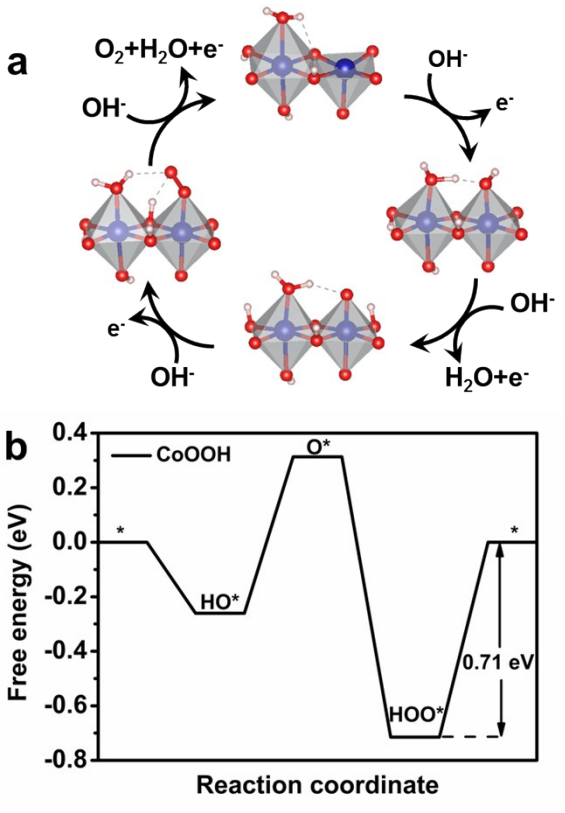

Fig. S8. (a) The optimized adsorption configurations of oxygen intermediates and (b) the calculated free energy change of OER sub-reactions under *U* = 1.23 V vs. RHE on edge site of CoOOH. The blue, red, and pink balls represent Co, O, and H atoms.

4. SEM image of $Ni(OH)_2$ nanosheet array

SEM image reveals the nanosheet array like moropholy of the as-prepared samples.

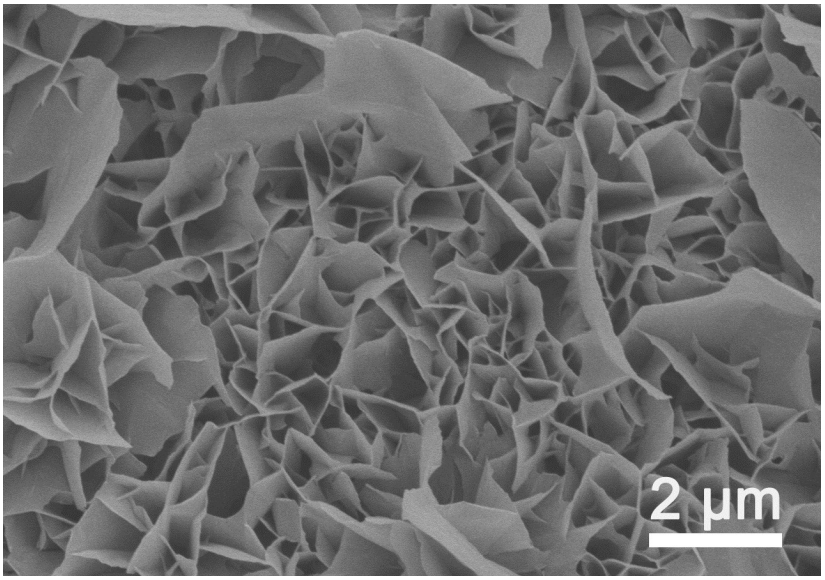

Fig. S9. Typical SEM image of the as-prepared $Ni(OH)_2$ nanosheet array.

References

1. Han, X.; Yu, Y.; Huang, Y.; Liu, D.; Zhang, B. Photogenerated Carriers Boost Water Splitting Activity over Transition-Metal/Semiconducting Metal Oxide Bifunctional Electrocatalysts. *ACS Catal.* **2017**, *7*, 6464-6470.
2. Kresse, G.; Furthmüller, J. Efficient Iterative Schemes for ab initio Total-energy Calculations Using a Plane-wave Basis Set. *Phys. Rev. B* **1996**, *54*, 11169-11186.
3. Kresse, G.; Joubert, D. From Ultrasoft Pseudopotentials to the Projector Augmented-Wave Method. *Phys. Rev. B* **1999**, *59*, 1758.
4. Perdew, J.; Burke, K.; Ernzerhof, M., Generalized Gradient Approximation Made Simple. *Phys. Rev. Lett.* **1996**, *77*, 3865-3868.
5. Dudarev, S.; Botton, G.; Savrasov, S.; Humphreys, C.; Sutton, A. Electron-energy-loss Spectra and the Structural Stability of Nickel Oxide: An LSDA+U Study. *Phys. Rev. B* **1998**, *57*, 1505-1509.
6. Grimme, S. Semiempirical GGA-type Density Functional Constructed with a Long-range Dispersion Correction. *J. Comput. Chem.* **2006**, *27*, 1787-1799.
7. Xiao, J.; Pan, X.; Guo, S.; Ren, P.; Bao, X. Towards Fundamentals of Confined Catalysis in Carbon Nanotubes. *J. Am. Chem. Soc.* **2015**, *137*, 477-482.
8. Wang, Z.; Liu, H.; Ge, R.; Ren, X.; Ren, J.; Yang, D.; Zhang, L.; Sun, X. Phosphorus-doped Co_3O_4 Nanowire Array: a Highly Efficient Bifunctional Electrocatalyst for Overall Water Splitting. *ACS Catal.* **2018**, *8*, 2236-2241.
9. Nørskov, J.; Rossmeisl, J.; Logadottir, A.; Lindqvist, L. Origin of the Overpotential for Oxygen Reduction at a Fuel-Cell Cathode. *J. Phys. Chem. B* **2004**, *108*, 17886-17892.
10. Huang, Z.; Song, J.; Du, Y.; Xi, S.; Dou, S.; Nsanzimana, J.; Wang, C.; Xu, Z.; Wang, X. Chemical and Structural Origin of Lattice Oxygen Oxidation in Co–Zn Oxyhydroxide Oxygen Evolution Electrocatalysts. *Nat. Energy* **2019**, *4*, 329-338.
11. Cai, Z.; Zhou, D.; Wang, M.; Bak, S.; Wu, Y.; Wu, Z.; Tian, Y.; Xiong, X.; Li, Y.; Liu, W.; Siahrostami, S.; Kuang, Y.; Yang, X.; Duan, H.; Feng, Z.; Wang, H.; Sun X. Introducing Fe^{2+} into Nickel–Iron Layered Double Hydroxide: Local Structure Modulated Water Oxidation Activity. *Angew. Chem. Int. Ed.* **2018**, *57*, 9392-9396.